THE JOURNAL OF PHYSICAL CHEMISTRY B

Article

pubs.acs.org/JPCB

Topological Origin of Fragility, Network Adaptation, and Rigidity and Stress Transitions in Especially Homogenized Nonstoichiometric Binary Ge_xS_{100-x} Glasses

Shibalik Chakraborty and P. Boolchand*

Department of Electronic and Computing Systems, College of Engineering and Applied Science, University of Cincinnati, Cincinnati, Ohio 45220-0030, United States

ABSTRACT: Binary Ge_xS_{100-x} glasses reveal a richness of elastic and chemical phase transitions driven by network topology. With increasing Ge content (x), well-defined rigidity at $x_c(1) = 19.3(5)\%$ and a stress transition at $x_c(2) = 24.9(5)\%$ are observed in Raman scattering. In modulated DSC measurements, the nonreversing enthalpy of relaxation at T_g reveals a square-well-like minimum (reversibility window) with window walls that coincide with the two elastic phase transitions. Molar volumes show a trapezoidal-like minimum (volumetric window) with edges that nearly coincide with the reversibility window. These optical, thermal, and volumetric results are consistent with an isostatically rigid elastic phase (intermediate phase, IP) present between the rigidity ($x_c(1)$) and stress ($x_c(2)$) transitions. Complex C_p measurements show melt fragility index, $m(x)$ to also show a global minimum in the reversibility window with $m < 20$, underscoring that melt dynamics encode the elastic behavior of the glass formed at T_g. The strong nature of melts formed in the IP has an important practical consequence; they lead to slow homogenization (over days not hours) of nonstoichiometric Ge−S batch compositions reacted at high temperatures. Homogenization of chalcogenide melts/glasses over a scale of a few micrometers is a prerequisite to observe the intrinsic physical properties of these materials.

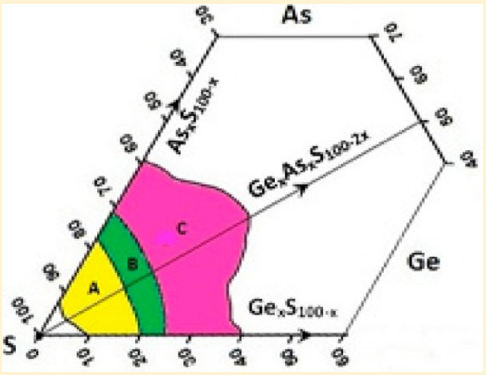

1. INTRODUCTION

Binary alloys of the Group IV (A = Si, Ge) with the Group VI (B = S, Se) elements, A_xB_{100-x} provide an attractive testing laboratory to explore the physics and chemistry of network glasses. The attraction derives from the extensive bulk glass forming range ($10\% < x < 44\%$) that permits probing glass molecular structure evolution with network topology. More importantly, these materials afford the unique opportunity to examine the nature of the Maxwell rigidity transition, which was predicted[1,2] to occur when the count of mechanical constraints due to bond-stretching and bond-bending forces per atom, $n_c = 3$, the degrees of freedom per atom in a 3D network. For an A_xB_{100-x} glass, since A atom is 4-fold and B is 2-fold coordinated, the count of mechanical constraints for atom A is 7 and for B is 2, and the $n_c = 3$ condition occurs when the A-atom content increases to $x = 20$ mol %. And as the field evolved, it was in the late 1990s when experiments first revealed the existence of two separate elastic phase transitions[3,4] in the Si−Se binary, a rigidity transition near $x = 20\%$ followed by a stress transition near $x = 26\%$ instead of a solitary Maxwell rigidity transition.[1,2,5] Here, x represents the mole% of Si. More recently, MD simulations on realistic glass structures confirm that picture.[6,7] The case of the Ge−Se binary[8−10] has also been studied, and two distinct and sharp elastic phase transitions, a rigidity (at $x_c(1) = 19.5(5)\%$) and a stress (at $x_c(2) = 26.0(5)\%$) transition followed by a chemical nanoscale phase separation (NSPS) transition near $x_c(3) = 31.5(5)\%$ are observed in glasses of proven homogeneity. Homopolar Ge−Ge bonds are first manifested in these glasses once at $x > x_c(3)$ and lead the chemical order of the stoichiometric $GeSe_2$ glass to be partially broken with a small (<2%) but finite concentration of homopolar bonds.[11,12] Given the close similarity of chemical bonding displayed by S and Se, one expects these transitions to be manifested in binary Ge_xS_{100-x} glasses as well. In this work, we provide the evidence for these elastic and chemical phase transitions. A key to observing the intrinsic physical behavior of these nonstoichiometric chalcogenides glasses is the need for homogeneous melts. Recent developments[9,10,13] to monitor melt heterogeneity in real time during synthesis using Raman scattering has greatly facilitated growth of homogeneous batch compositions on a scale of 5 μm or less.

Why does one observe two elastic phase transitions instead of one Maxwell rigidity transition? Isostatically rigid networks form at the Maxwell rigidity transition. These are networks for which the count of mechanical constraints due to bond-stretching and bond-bending forces per atom, n_c equals 3, the degrees of freedom per atom.[10,14] Isostatically rigid networks can lower their free energy by reconnecting, to expel mutually incompatible bonds that create stress[14,15] and thereby upshift the stress transition, thus, opening an intermediate phase[10,16]

Received: December 2, 2013
Revised: January 27, 2014
Published: January 28, 2014

   dx.doi.org/10.1021/jp411823j | J. Phys. Chem. B 2014, 118, 2249−2263

provided networks possess appropriate ring structures.[6] The nature of networks populated in the intermediate phase (IP) is quite special; they are rigid but unstressed,[17] aging is qualitatively suppressed in them, they display thermally reversing glass transitions,[18−21] they fill space efficiently, and they possess the property to reconnect or adapt.[22] The feature of adaptation was elegantly demonstrated in the IP of a triangular lattice.[23,24] Intermediate phases have been observed in modified oxides,[25] heavy metal oxides,[26] and solid electrolyte glasses[27] with profound consequences on electrical transport.[28] Here we will show that these universal features associated with the IP are also observed in the present Ge−S binary glasses.

The molecular structure of binary Ge−S glasses has been examined since the early 1970s.[29−32] In early work the glass forming ranges were identified.[32] There is general recognition that in S-rich glasses (x < 12%), S_8 rings form and segregate from the glassy Ge−S backbone.[29−31,33] At higher concentrations (x > 12%), an ordered bond network (OBN) of Ge cross-linked S_n chains emerges as revealed from the transverse optic IR reflectance response.[29] The authors observed the F_2 mode strength of GeS_4 tetrahedra to increase linearly with Ge content in the 15% < x < 33.3% range in harmony with OBN model but not a random covalent network.[34] More recently, Takebe et al.[30] and separately Cai and Boolchand[35] recognized the difficulty in obtaining homogeneous glasses by reaction of starting materials (Ge, S) at elevated temperatures (950 °C) for up to 48 h. Variations in Ge stoichiometry across a batch composition can be quite high, as large as 3−5%. Such variations will hinder observing the IP.[36] Neutron[31,37] and high energy X-ray scattering results on Ge−S binary glasses have placed the fraction of edge-sharing (ES) to corner-sharing (CS) tetrahedra near 0.44(3)[31] and 0.47(5)[37] for the stoichiometric glass GeS_2. Homogeneous glasses at the stoichiometric composition, in principle, can be grown more easily because of the existence of underlying crystalline phases that speed up kinetics of melt homogenization. However, for nonstoichiometric melts/glasses, homogenization is a far more challenging issue as we will address in the present work. Not surprisingly, results from various groups on these nonstoichiometric compositions display significant variations,[29−34] and we comment on the issue in the present work.

In section 2, we address bulk glass synthesis issues and the experimental methods used to characterize them. In section 3 we provide the experimental results. This is followed by section 4 on discussion of salient issues. Conclusions are summarized in section 5.

2. MATERIALS AND METHODS

2.1. Synthesis of Melts/Glasses. Dry elemental Ge and S lumps of 99.999% purity from Strem Chemicals Inc. and Cerac Inc., respectively, were encapsulated in evacuated (~2 × 10^{-7} Torr) 5 mm ID quartz tubings. Elemental sulfur platelets were vacuum desorbed on a high vacuum pumping line for 24 h prior to use. The elements were reacted at temperatures ranging from 700 to 950 °C in a T-regulated box furnace, depending on the composition, from periods ranging from 1 day < T_R < 21 days. Care was taken to increase the furnace T at a 1/2 °C/min ramp rate to permit S and Ge to react so that elemental S-rich regions do not lead to explosion of ampules. Batch sizes were kept at 1.50 g. Fused quartz tubes were washed using ammonium bifluoride and then rinsed in DI water. Tubes were then dried in a vacuum oven (90 °C) for 24 h before use. Periodically, melts were water quenched and FT-Raman spectra taken along the length of a melt column. The process of FT-Raman profiling was continued until all spectra taken along the length of the melt column became identical. At that point we took batch compositions to be homogeneous. The typical reaction time T_R to homogenize 1.50 g sized melts in the indicated T range was found to be nearly 21 days.

2.2. FT Raman Scattering. The Raman profiling method[9,13] used a Thermo-Nicolet Model Nexus 870 FTIR system with a Raman Module accessory to record spectra of glasses. The Raman module has a motorized stage on which bulk glasses encased in quartz tube were mounted, and spectra were acquired at a select number of locations and spacing along a melt column specified by software. A typical measurement at one location involved 300 scans, gave a 2 cm^{-1} resolution, and took 12 min accumulation time. In these experiments, scattering was excited using 100 mW of 1064 nm radiation from a Nd:YAG laser with a 50 μm spot size, and the radiation was brought to a focus at the interface between the quartz tubing and the Ge−S bulk glass wetting it. Spectra were acquired at eight locations spaced 2 mm apart to cover a 20 mm long melt column. These spectra were superimposed to give a pictorial view of melt heterogeneity as reflected in the varying stoichiometry of the glass specimen sampled locally by the laser beam. To ascertain the homogeneity of bulk glasses so homogenized, they were separately investigated at a higher spatial resolution of 2 μm using a Micro-Raman system. The details of the method are provided below.

2.3. Dispersive Raman Scattering. A triple monochromator model T64000 from Horiba Jobin Yvon Inc. was used to establish the vibrational density of states and probe the molecular structure of the homogenized glasses. The instrument was operated in a triple subtractive mode using a CCD detector. A majority of our Raman dispersive measurements on homogeneous glasses were performed in the macro-mode, using 5 mWatts of 514 nm exciting radiation from an Ar-ion laser with a 50 μm laser spot size. In these experiments we followed a strict protocol by rigorously controlling three conditions: (i) the laser power-density was kept fixed (optically controlled) at 0.04 W/cm^2 at all compositions, (ii) scattering was examined with glass samples always wetting and sealed in the synthesis quartz tube that was evacuated (10^{-7} Torr), and (iii) laser light was bought naturally to a line focus at the quartz tube/Ge−S glass interface, further reducing the power density.[9] The laser beam was focused on the quartz−glass sample interface using an XY stage in the macro-chamber to optimize signal. The reduced laser power density facilitated suppressing photostructural effects,[34,38] and to capture the quiescent mode scattering strength variations with x. The planarity of the quartz−Ge−S glass interface, the small (50 μm) laser spot size, homogeneity of glass samples led to Raman lineshapes that were independent of probe beam location along the melt column.

In select cases, we also undertook micro-Raman dispersive measurements on bulk glasses to ascertain their homogeneity on a spatial resolution of 2 μm using an Olympus Model BX41 microscope attachment with an 80× objective. These experiments were undertaken to complement the FT-Raman profiling experiments on batch compositions. They revealed that once melts were homogenized to a scale of 50 μm in the FT-Raman experiments, they were actually homogeneous on a much finer scale of about 2 μm. We provide an example in the next section.

2.4. Scanning Calorimetry. *2.4.1. Modulated Differential Scanning Calorimetry.* Once Raman scattering measurements

were completed, glass ampules were broken open and about 0.020 g of each glass composition hermetically sealed in Al pans for modulated DSC experiments. We used a model 2920 MDSC from TA Instruments Inc. operated at 3 °C/min scan rate, and sinusoidal modulation amplitude kept at 1 °C, and a modulation period of 100 s. We established T_g from the inflection point of the reversing heat flow and, separately, the enthalpy of relaxation (ΔH_{nr}) at T_g from the nonreversing heat flow. By recording scans in heating, followed by the cooling cycle, the frequency corrected[20,39] nonreversing enthalpy was established. At select glass compositions we also compared the glass transition endotherm in an MDSC mode with one in DSC mode. From these scans we could deduce T_g, ΔH_{nr}, and ΔC_p as a function of glass composition. To ascertain reproducibility of data, a minimum of two samples were investigated at each composition.

2.4.2. AC Calorimetric Measurements. A model Q2000 DSC from T.A. Instruments Inc., operated in the MDSC mode with the glass transition endotherm analyzed in terms of complex specific heat C_p was used to establish the fragility of melts. The out-of-phase C_p shows[40−42] a peak near T_g, while the in-phase component of C_p shows[40,41] a rounded step. At the peak location of the out-of-phase C_p component, the glassy system completely tracks the modulated heat flow, that is, $\omega\tau = 1$, where ω represents the modulation frequency and τ is the enthalpy relaxation time. In a typical measurement, five different modulation frequencies ω ($=2\pi/T_\omega$) were used (with time periods T_ω ranging from 60 to 120 s). These AC calorimetric measurements make use of the fact that as ω increases, the peak of the out-of-phase C_p shifts to higher T. By measuring τ as a function of T and making a plot of log τ against T_g/T, we extracted the fragility index "m" using eq 1.

$$m = \lim_{T \to T_g} \left| \frac{\mathrm{d} \log \tau}{\mathrm{d}(T_g/T)} \right| \quad (1)$$

The compositional variation of the fragility index $m(x)$ was established, and these data will be presented in the next section.

2.5. Volumetric Measurements. The density of glasses was measured using a hooked quartz fiber suspended from a digital microbalance (with 0.001g resolution). Samples were weighed in air and then in 200 proof alcohol, and using Archimedes' principle, we obtained density using eq 2. The density of ethyl alcohol was calibrated by using a Si single crystal standard (ρ_{Si} = 2.329 g/cm^3).

$$\rho_{sample} = [\mathrm{mass}_{air}/(\mathrm{mass}_{air} - \mathrm{mass}_{alcohol})]x\rho_{alcohol} \quad (2)$$

By using glass samples of 0.150 g in size or more we could establish the density to an accuracy of 1/4%. The accuracy of the measurements were independently ascertained by measuring the density of a Ge single crystal that is known to be ρ_{Ge} = 5.323 g/cm^3. Molar volumes were then obtained by inverting the densities and multiplying with the individual molar masses.

3. EXPERIMENTAL RESULTS

3.1. Kinetics of Melt Homogenization from FT-Raman Scattering. Figure.1 provides a typical example of a Raman profiled measurement of a quenched melt at x = 30%, taken after reaction of the starting materials for T_R = 4, 9, and 21 days, respectively. A perusal of the observed lineshapes shows the vibrational spectra vary significantly along the melt column

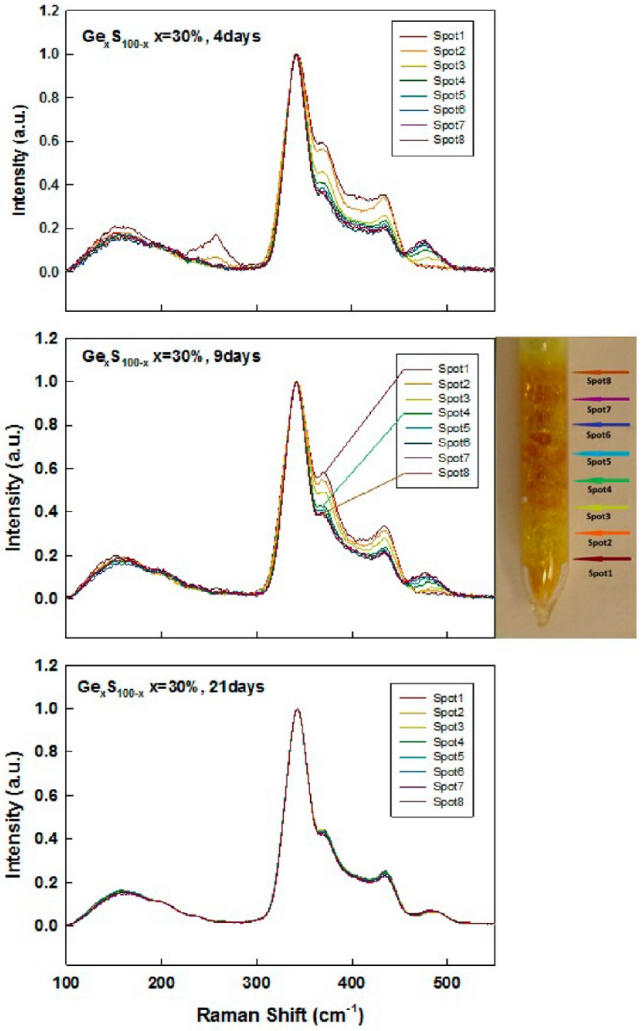

Figure 1. FT-Raman profile of a $Ge_{30}S_{70}$ glass sample of 1.50 g in size taken after 4, 9, and 21 days of reaction of starting materials. In the 4-day sample, the mode near 260 cm^{-1} is evidence of a Ge-rich species (ethane-like units). After 21 days of reaction, all eight Raman lineshapes coincided, showing that the batch composition has homogenized. The picture is an actual glass sample encased in quartz tubing shown next to the middle panel with the eight locations where Raman spectra were recorded shown by arrows. Note that spot 1 is the lowest and 8 is the highest, and after 8 days of reaction spot 1 continues to be a Ge-rich glass.

at T = 4 days but that variation steadily diminishes and eventually vanishes after T_R = 21 days.

A fully homogeneous melt was thus obtained after 21 days of reaction of the starting materials for the 1.5 g sample (Figure 1), but only after 10 days for a smaller-sized 0.50 g sample (Figure 2). These data suggest that the underlying kinetics of homogenization is diffusion controlled, an issue we will discuss in section 4.2. In general, Ge−S melts of 1.50 g in size took 21 days to homogenize.[43] The corresponding Ge−Se batch compositions of 2.00 g in size took 7 days to homogenize.[9,13,44]

Thus, slow homogenization of these nonstoichiometric chalcogenide batch compositions appear to be a generic feature, and we shall comment on the microscopic origin in section 4.2.

3.2. Dispersive Raman Scattering. *3.2.1. Melt Homogenization Probed in Dispersive Micro-Raman Scattering.* Figure 3 shows an example of a FT-Raman profiled

dx.doi.org/10.1021/jp411823j | J. Phys. Chem. B 2014, 118, 2249−2263

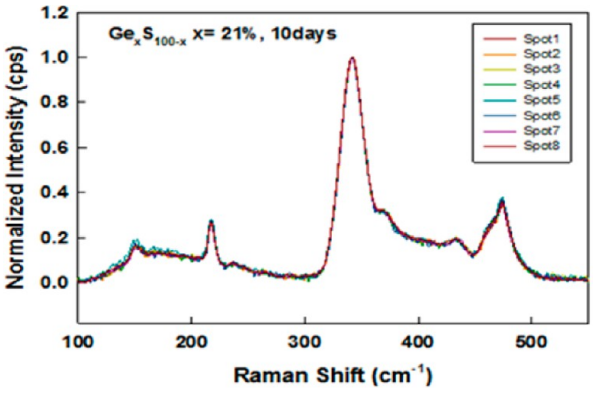

Figure 2. FT Raman profile of a 0.50 g glass of $Ge_{21}S_{79}$ showing complete homogeneity after being reacted for 10 days. Smaller batch sizes homogenize quicker, underscoring a diffusion-assisted mixing of melts.

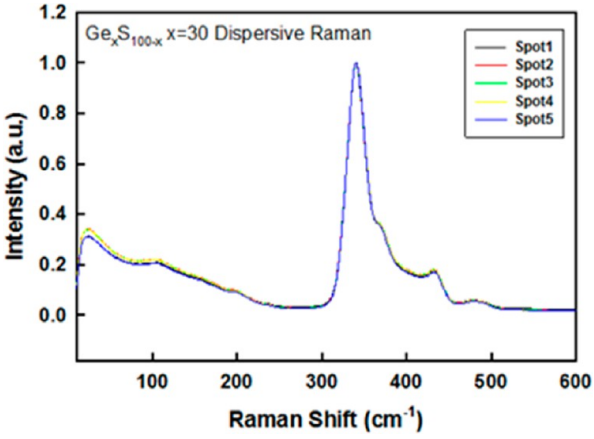

Figure 3. Dispersive Micro-Raman scattering data on a $Ge_{30}S_{70}$ sample taken at 5 points along the length of a quartz ampule showing it to be homogeneous on a scale of 2 μm as well.

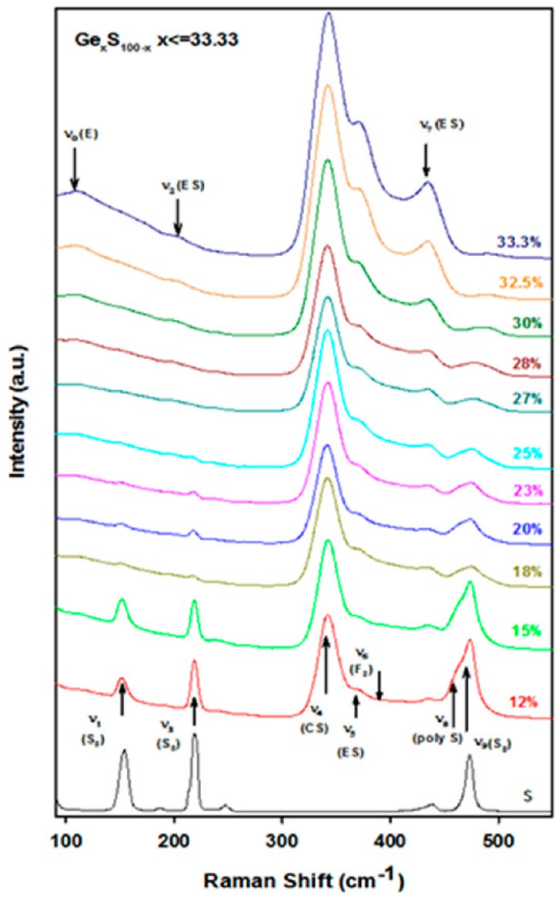

Figure 4. Dispersive macro-Raman spectra of 11 homogenized Ge_xS_{100-x} glass compositions ($12\% < x < 33.3\%$) showing line shape evolution with composition (x). See text for assignments of the nine modes indicated. For reference, the bottom most spectrum is that of orthorhombic sulfur.

homogeneous bulk glass that was then examined in a Micro-Raman dispersive system. In such a system, the laser beam was brought to a tight focus with a spot size of 2 μm. Here we see that by recording spectra at several locations we could not detect any measurable heterogeneity on a scale of 2 μm, suggesting that, once batch compositions were homogenized in the FT-Raman scattering measurements on a scale of 50 μm, they were actually homogeneous on a finer spatial scale of about 2 μm.

3.2.2. Glass Structure using Dispersive Macro-Raman Scattering. We examined 11 glass compositions varying in Ge content from $12\% < x < 33.33\%$, and the Raman results are summarized in Figure 4. For comparison, we have included Raman spectrum of elemental S at the bottom of the panel. The Raman spectra reveal rich line shapes broadly composed of nine modes labeled ν_1–ν_9. The present Raman results are qualitatively similar to previous reports in the field, and there is broad agreement on the assignment of the modes as well.[31,33,34,38,45] The assignments have been facilitated by numerical simulations on ab initio cluster calculations[46] and also MD simulations on glasses.[47] However, when one compares details of the line shape analysis, such as mode-frequency and mode-scattering strength variation with composition, striking differences appear from earlier reports. We shall discuss these data comprehensively in section 4.5. The mode assignments can be briefly summarized as follows: corner sharing (340 cm^{-1}), edge sharing (203, 373, and 436 cm^{-1}), tetrahedra of GeS_4, S_8 ring modes (147, 217, and 471 cm^{-1}), and S_n-chain mode (460 cm^{-1}). The observed spectra were deconvoluted as a superposition of Voight line shapes (Gaussian–Lorentzian mix with the ratio kept constant) using "Peak fit" software.[48] In such a nonlinear least-squares fitting routine, mode-frequency, mode-scattering strength, and mode-FWHM were kept as variables. There are three vibrational modes of central importance that serve to define not only the glass structure evolution as the S_n chain network is steadily cross-linked by Ge but also the underlying evolution of elastic phases. These three modes of interest include the CS and ES modes of GeS_4 tetrahedra, and polymeric S_n chain mode. Analysis of the Raman results show that frequency of the GeS_4 corner-sharing (CS) mode (ν_4) near 340 cm^{-1}, and that of the ES mode (ν_5) near ν = 373 cm^{-1}, steadily blue-shift with increasing Ge content of glasses (Figure 5). The observed blue-shift in the CS and ES modes displays kinks near Ge content $x_c(1)$ = 19.3(5)% and $x_c(2)$ = 24.9(5). These kinks will be related to the two elastic phase transitions, rigidity and stress, respectively (section 4.1). Furthermore, the underlying optical elasticity power laws deduced from the mode frequency squared (ν^2_{CS}, ν^2_{ES}) variation will uniquely serve to establish the nature of the underlying elastic phases (section 4.1). From the observed mode scattering strength variation of the CS and

dx.doi.org/10.1021/jp411823j | J. Phys. Chem. B 2014, 118, 2249–2263

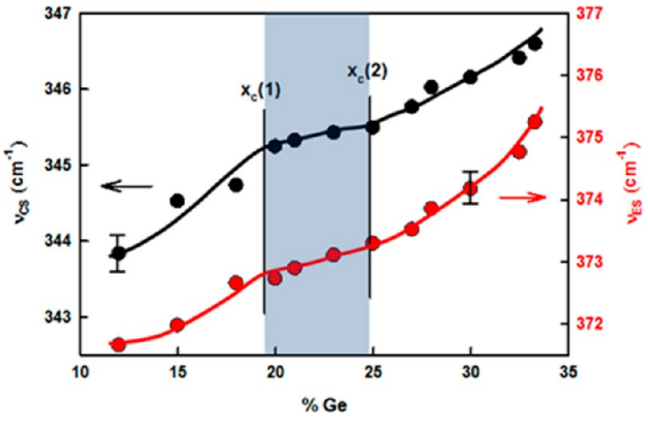

Figure 5. Corner sharing (CS) and edge sharing (ES) modes blue shift as a function of Ge content. These data have permitted extracting the two elastic phase transitions at $x_c(1)$ = 19.3(5)% (rigidity) and $x_c(2)$ = 24.9(5) (stress). The blue shaded region between these two transitions represents the intermediate phase (IP).

ES modes, vital information on the evolution of the glass network structure will emerge and is comprehensively discussed in section 4.4.

3.3. Glass Transition Temperature (T_g), Non-Reversing Enthalpy of Relaxation at T_g, and Specific Heat Jump at T_g. In Figure 6 we show an example of an MDSC scan and a

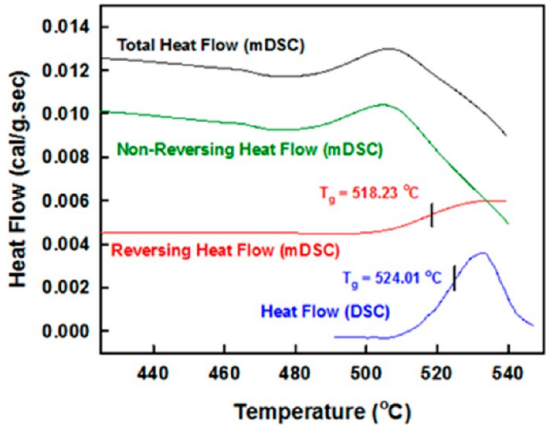

Figure 6. Modulated DSC scan taken at 3 °C/min scan rate, showing the total heat flow (black). The nonreversing heat flow (green) and the reversing heat flow (red) for a GeS_2 glass. From the inflection point of the total heat flow, a T_g = 518.2 °C is deduced. In a DSC scan at 10 °C/min, from the inflection point of the heat flow endotherm (blue), we obtained a T_g of 524 °C.

DSC scan for the case of the stoichiometric GeS_2 glass. The top three scans show respectively the total, nonreversing, and the reversing heat flow from an MDSC scan. From the inflection point of the reversing heat flow we obtain a T_g of 518(2) °C. A DSC scan (lowest scan in Figure 6) of the same glass sample taken at a scan rate of 10 °C/min shows an endotherm from which we deduce a T_g of 524(2) °C from the inflection point. In Figure 7 we compare the T_g of GeS_2 glass from the present work with those reported earlier. Our DSC deduced T_g of 524(2) °C may be compared to the value of 493.3 °C reported by Malek et al.,[49] to a value of 495.2 °C by Bychkov et al.[31] Our MDSC deduced T_g of 518 °C may be compared to a value of 514 °C reported by Zeidler et al.[37] and 508 °C reported by Cai and Boolchand.[35] Once again, the spread in T_g can be

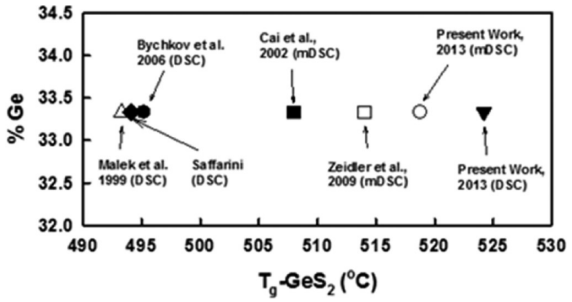

Figure 7. Comparison of T_g of GeS_2 glass from different reports; present work (524 °C (▼) and 518 °C (○)) and earlier reports (Malek et al.[49] −493.3 °C (Δ), Bychkov et al.[31] −495.2 °C (●), Cai et al.[35] −508.0 °C (■) and Zeidler et al.[37] −514 °C (□)).

attributed to glass heterogeneity by virtue of synthesis, as noted for solid electrolyte glasses[27] earlier.

A summary of mDSC results showing compositional variation of $T_g(x)$, $\Delta H_{nr}(x)$, and $\Delta C_p(x)$ in the present Ge−S binary are summarized in Figure 8. $T_g(x)$ shows an increase with x (Figure 8a), a behavior that is consistent with an increased cross-linking of the backbone.[50] In the same figure we have also included a plot of the slope of T_g with x, dT_g/dx and find that it displays a maximum near x = 31%. The slope dT_g/dx was established by averaging data on four adjacent compositions. $T_g(x)$ shows a maximum near x = 33.3% Ge and decreases at higher x. The slope dT_g/dx revealed a maximum near x = 31%, which we suggest represents the onset of Ge−Ge bond formation in the Ge−S glasses as nanoscale phase separation (NSPS) ensues and slows down the growth of $T_g(x)$. In Figure 8b, we plot the variation in $\Delta H_{nr}(x)$ and find the term displays a global minimum in the 20% < x < 25% range with an almost square-well like behavior, and with the $\Delta H_{nr}(x)$ term increasing by an order of magnitude outside that range. The vanishing of $\Delta H_{nr}(x)$ is evidence of networks becoming isostatic.[19] Near x = 25%, one finds the window wall sharpens upon aging, but the reverse is the case near x = 20%. The latter behavior can be traced to growth of S_8 rings upon aging, as will be discussed in section 4.3.

For the readers convenience, we have included in Figure 8b DSC $T_g(x)$ results reported by Bychkov et al. These data clearly show that at x < 18%, the present results on T_g are quite similar to those of Bychkov et al.,[31] but at higher Ge concentrations such is not the case, most likely due to differences in sample make up, particularly their heterogeneity (section 4.5).

3.4. Variation of Fragility Index with Glass Composition. A perusal of the literature reveals that fragility index of melts typically vary from 20 for strong to almost 175 for fragile ones.[51] The variation of fragility index $m(x)$ in the present Ge−S melts (Figure 9) shows a broad minimum with m < 20 in the reversibility window (blue panel). A parallel behavior was observed in corresponding Ge−Se glasses.[40] Clearly melt dynamics and nonreversing enthalpy of relaxation at T_g in glasses are closely correlated to network topology. Of special interest is the composition x = 25% for which m shows a global minimum of 15.2(4), measurably lower than the value of 20 for the archetypical strong melt of SiO_2.[52] Such a superstrong melt will serve as a barrier in atomic scale mixing of the starting materials as they are reacted at 950 °C, leading to slow homogenization of batch compositions (section 4.2).

3.5. Variation of Molar Volumes of Ge−S Glasses with Composition and Aging. A plot of the variation in molar

dx.doi.org/10.1021/jp411823j | J. Phys. Chem. B 2014, 118, 2249−2263

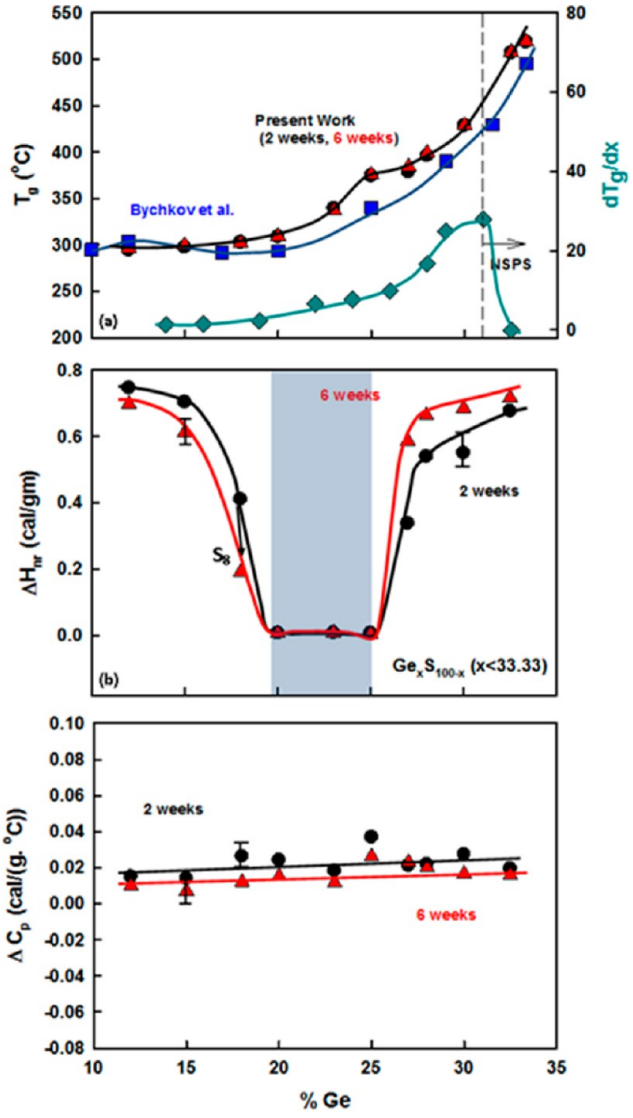

Figure 8. Variation in (a) glass transition temperature $T_g(x)$, and (b) enthalpy of relaxation at T_g, $\Delta H_{nr}(x)$, showing the reversibility window as the blue panel. The slope of dT_g/dx is included in panel (a) and shows a maximum near $x = 31\%$ corresponds to the nanoscale phase transition. Glass compositions at $x > 31\%$, are found to segregate into S-rich and Ge-rich (Ge_2S_3) nanophases. In (c) we plot variation in the specific heat jump, $\Delta C_p(x)$ at T_g and find the term to be independent of x.

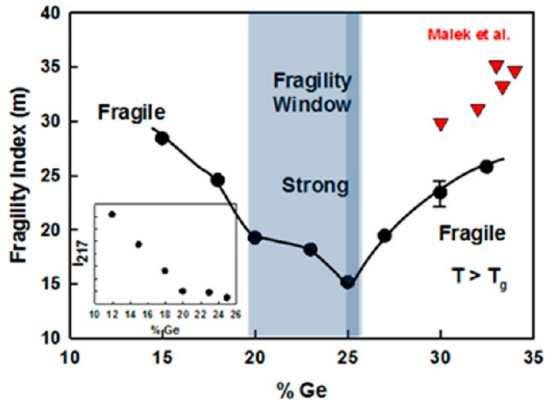

Figure 9. Variation in the fragility index $m(x)$ in Ge_xS_{100-x} glasses as a function of x. Note that $m(x)$ becomes less than 20 in the blue panel, the reversibility window from Figure 8. The measurements also reveal an $m = 15.2$ near $x = 25\%$, indicating a superstrong melt composition, dark blue band. At this composition, the concentration of S_8 rings vanishes. The inset plots the scattering strength of the 217 cm^{-1} S_8 mode variation with glass composition. The superstrong melt composition will serve as a diffusive barrier in melt mixing.

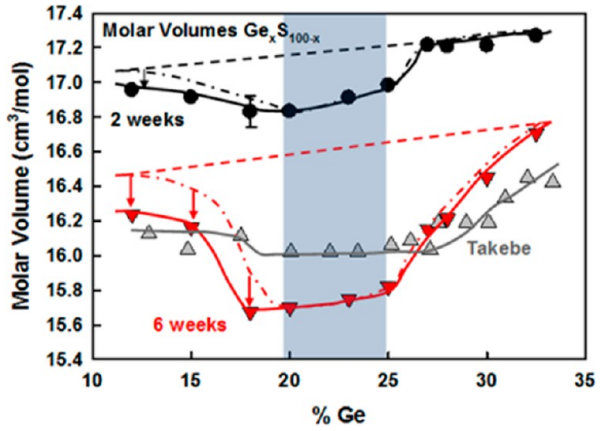

Figure 10. Variation of in molar volume $V_m(x)$ with composition in the Ge−S binary studied after 2 and 6 weeks of aging. Note that $V_m(x)$ decreases as glassy networks relax at room temperature. The compaction of glasses in general is driven by long-range forces. The work of Takabe et al. is taken from ref 30.

volumes, $V_m(x)$, measured on 2 week aged glasses at 300 K show a mild minimum at $x < 27\%$, which gets strikingly deeper as glasses age to 6 weeks (Figure 10). These data demonstrate that IP glass compositions, such as for example at $x = 25\%$ composition, compact nearly 7% upon aging, while the one near $x = 30\%$, outside the IP, shows only a 4.0% compaction in V_m.

It is widely known[31,33] that binary Ge−S glasses containing less than 25% of Ge have a finite concentration of S_8 rings (Figure 9, inset) and that their concentration steadily increases as these glasses age. We illustrate the result for the case of a glass at $x = 15\%$ in Figure 11, which shows Raman scattering taken after a 2 week and after a 6 week waiting time. Modes characteristic of S_8 rings near 147, 220, and 470 cm^{-1} increase in scattering strength upon aging. Thus, to schematically separate the effect of aging of the backbone from the strictly chemical segregation of S_8 rings, we have drawn a rough broken line curve that provides our estimate of $V_m(x)$ due to aging of the glassy backbone. We shall discuss these results in section 4.3.

4. DISCUSSION

4.1. Rigidity Theory, Topology, and the Three Elastic Phases in Ge−S Glasses. The optical, calorimetric, and volumetric studies on the present glasses each display three distinct regimes of variation. We have already noted in Raman scattering that the CS and ES mode frequency display thresholds near $x = x_c(1) = 19.3(5)\%$ and $x = x_c(2) = 24.9(5)\%$ (Figure 5). In the calorimetric measurements, the enthalpy of relaxation near T_g displayed a square-well like reversibility window (Figure 8b) with walls near $x_c(1)$ and $x_c(2)$. Finally, molar volumes of the glasses display a minimum, trapezoidal volumetric window (Figure 10) with edges located near $x_c(1)$ and $x_c(2)$. The privileged role of the IP glass composition in the $x_c(1) < x < x_c(2)$ range has thus emerged

dx.doi.org/10.1021/jp411823j | J. Phys. Chem. B 2014, 118, 2249−2263

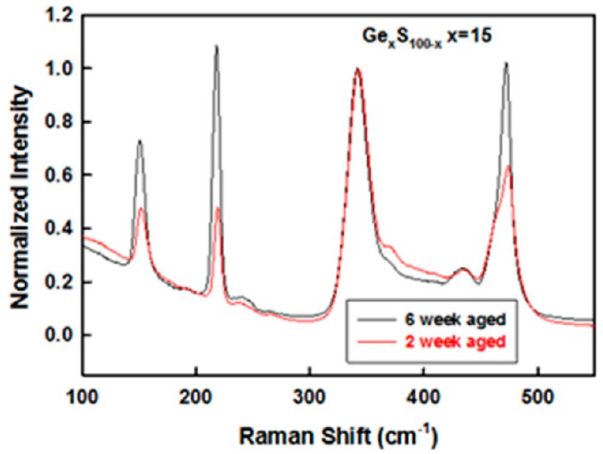

Figure 11. Raman spectrum of a $Ge_{15}S_{85}$ glass taken 2 weeks and 6 weeks after melt quenching, showing growth of S_8 rings modes upon aging. Decoupling of S_8 rings is a feature observed in S-rich ($x < 20\%$) glasses.

from three diverse experiments. These data raise basic issues, what do these two thresholds represent? What is the nature of the three elastic phases delineated by these two thresholds? In this section we now show that the compositions $x_c(1)$ and $x_c(2)$ represent the rigidity and stress transitions, respectively, and that glasses at $x < x_c(1)$ are in the flexible phase and, with increased cross-linking, enter in the isostatically rigid phase, $x_c(1) < x < x_c(2)$, and, at $x > x_c(2)$, the stressed-rigid elastic phase.

Perhaps one of the most attractive aspects of rigidity theory of glasses is its predictive power. Numerical simulations[53,54] on amorphous networks possessing a connectivity $\langle r \rangle$ that exceeds the Maxwell Rigidity transition reveal that their elasticity (C) increases as a power law,

$$C - C_o = A(\langle r \rangle - \langle r_c \rangle)^p \quad (3)$$

Here, C represents the elasticity at a given $\langle r \rangle$, C_o is the threshold value of elasticity at $\langle r \rangle = \langle r_c \rangle$ corresponding to the Maxwell rigidity threshold, and p the elastic power law, with a value in the 1.4 to 1.5 range for 3D networks. In Raman scattering, glasses were studied at discrete compositions. On the other hand, elastic thresholds need not necessarily occur at discrete compositions. The question then remains, how does one accurately derive the elastic thresholds? We use an iterative method to derive the points at which the threshold occurs. With a set of Raman mode frequency shifts ν_1, ν_2, ..., ν_n at glass compositions r_1, r_2, ..., r_n, we extracted the optical elastic power law "p" and elastic threshold composition "x_c" as follows. In the Raman experiments, the mode frequency squared provides a measure of an optical elasticity, since $\nu^2 = k/m$, where k is an effective spring constant and m the atomic mass. So that one writes eq 3 equivalently as eq 4,

$$\nu^2 - \nu_c^2 = A(\langle r \rangle - \langle r_c \rangle)^p \quad (4)$$

where ν_c represents the value of ν at the elastic threshold composition $\langle r_c \rangle$. Using this equation, we can either employ a linear fit directly to the eq 4 or, alternatively, a linear fit to eq 5.

$$\ln(\nu^2 - \nu_c^2) = \ln A + p \ln(\langle r \rangle - \langle r_c \rangle) \quad (5)$$

In binary Ge_xS_{100-x} glasses, at $x < 33.3\%$, since the coordination of Ge and S are known to be 4 and 2, respectively, one can write the mean coordination number $\langle r \rangle = 4x + 2(1 - x)$ or $=2(1 + x)$. To evaluate the threshold, a starting composition x_c is chosen suggested by the Raman scattering experiments (Figure 5) and the its value iterated by small amounts to determine a power-law "p" using both methods. The final value of x_c was fixed when elastic power law determined using the two methods converged to the same value of "p". We have performed these calculations[43,44] from the available Raman mode frequency data and find for glasses in the 19 to 25% range, the rigidity transition ($x_c(1)$) occurs near 19.3(5)%, and for glasses in the 25 to 33.3% range, the stress transition ($x_c(2)$) occurs near 24.9(5)%. The elastic power laws for the IP and the SR phase are listed in Table 1.

Table 1. Optical Elastic Power Laws for the Intermediate and Stressed-Rigid Phases from Raman CS Mode Frequency Variation in the Ge−S Binary Compared with the Ge−Se Binary[9,10]

glass system	elas. power law; P_{int}	elas. power law; P_{SR}	rigidity trans.; $x_c(1)$	stress trans.; $x_c(2)$
Ge−S	1.00(1)	1.32(4)	19.3(5)	24.9(5)
Ge−Se	1.10(1)	1.47(3)	19.5(3)	26.03(3)

The IP between the rigid and the stress transition is characterized by an elastic power law of 1.0, while glasses at $x > x_c(2)$ are in the stressed-rigid phase possessing an elastic power law of 1.32(4) in excellent agreement with the numerical predictions of He and Thorpe.[53] The vibrational thresholds, that is, the rigidity and stress transitions, are accurately determined by Raman scattering and found to coincide with the calorimetric thresholds, that is, walls of the reversibility window (Figure 8b) and almost nearly so with the walls of the volumetric window (Figure 10). The low end of the reversibility and volumetric windows are altered by aging induced segregation of S_8 rings from the network backbone as will be discussed in section 4.3.

The results for the Ge−S binary glasses are compared with those in the Ge−Se binary (Table 1), and it is comforting to see that not only are the elastic power laws in both systems are remarkably similar, but the rigidity and stress transitions occur nearly at the same Ge content in respective binaries. These data underscore the similarity of glass molecular structure, as we discuss later.

Substantial efforts to characterize the IP have been made by topological analysis.[21] Currently there is no numerical prediction for the elastic power law in the intermediate phase, although not because of a lack of trying.

4.2. Melt Dynamics, Glass Elastic Behavior, and Slow Melt Homogenization. The predictive power of the Rigidity Theory appears not merely confined to the three generic elastic phases of glasses, but there is growing evidence that it extends to the dynamics of the parent melts from where these evolve.

4.2.1. Melt Dynamics Encode Glass Elastic Behavior. As a melt is supercooled, one has often wondered if melt dynamics would encode the nature of the glass formed at T_g. We are now in a position to comment on this fundamental issue. The archetypal SiO_2 glass is widely regarded as a strong glass with $m = 20$. As shown in Figure 12b, the fragility index of melts in the $20\% < x < 25\%$ range, the intermediate phase, are all lower than 20, that is, these melt compositions are superstrong.[40,55] Upon comparing the data of Figure 12b with 12c, one recognizes the exceptional properties of IP compositions; the melt fragility minimum coincides with the glass reversibility window. We

dx.doi.org/10.1021/jp411823j | J. Phys. Chem. B 2014, 118, 2249−2263

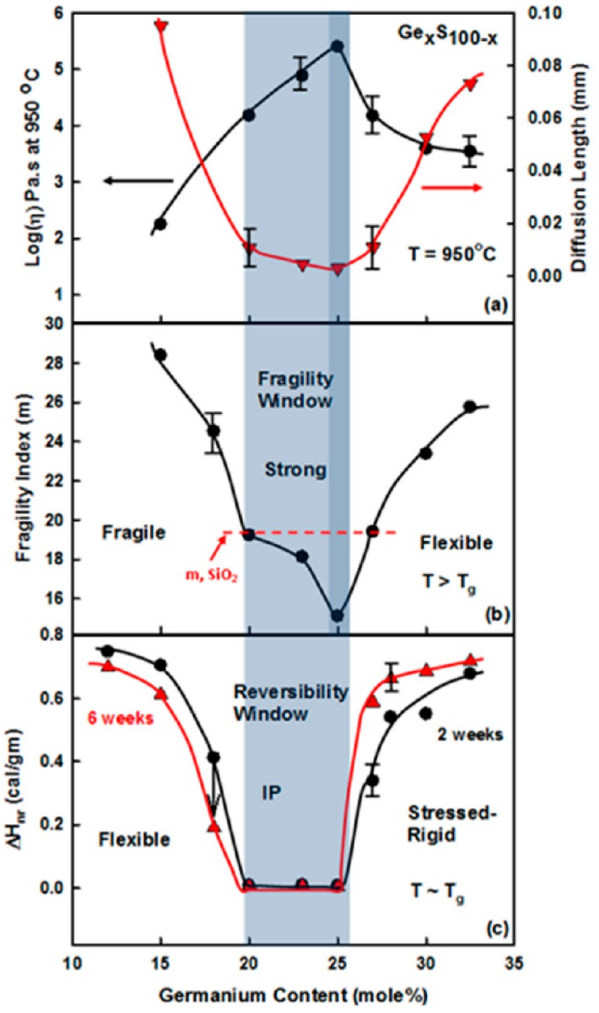

Figure 12. (a) Calculated variations of melt viscosity $\eta(x)$ and diffusion lengths $L(x)$ after 1 day of reaction at 950 °C from measured fragility index $m(x)$ near T_g, using the MYEGA approach. The VTF and MYEGA approaches yielded variations in $\eta(x)$ and $L(x)$ that were almost identical. (b) Variation in fragility index $m(x)$ from complex C_p measurements. (c) Variation in nonreversing enthalpy of relaxation at T_g, $\Delta H_{nr}(x)$, obtained 2 and 6 weeks after melt quenching. In (c) the segregation of S_8 rings from the backbone upon aging leads to a lowering of the $\Delta H_{nr}(x)$ term at $x < 20\%$. See section 4.3.

note (Figure.12b) that melts in the composition range $20\% < x < 27\%$ possess a lower fragility index $m(x)$ than the archetypal strong SiO_2 melt. These select superstrong melt compositions define a low fragility range (window) and note in passing that it almost coincides with the reversibility window (Figure 12c) characteristic of isostatically rigid glasses. Thus, in the present Ge−S binary melt dynamics described by fragility index actually encodes the elastic behavior of the resulting glass that forms at T_g. On the other hand, fragile melts can either give rise to elastically flexible glasses or stressed rigid ones. However, in the former m (Figure 12b) decreases with increasing T_g (Figure 8a), while in the latter m increases with T_g. Indeed, the scaling relationship between m and T_g with two distinct slopes, a positive and a negative one, is also observed in corresponding Ge−Se glasses[40,56] and will not be discussed further in this work.

4.2.2. Topology, Melt Fragility, and Slow Homogenization of Batch Compositions. William-Landel and Ferry[57] first characterized the viscous slowdown of melts as they are cooled to T_g by plotting the log of viscosity (η) against $1/T$, a phenomenology that was subsequently popularized by A. Angell.[58] Vogel, Fulcher, and Tammann[59] recognized that the dynamics of slowdown in different glasses can be characterized by a family of universal plots with the slope of $d(\log \eta)/d(T_g/T)$ near $T = T_g$ defining their overall shape. On such plots, melts displaying an Arrhenian behavior are viewed as strong, while those showing a bowing of the $\eta(T_g/T)$ curve are viewed as fragile.[58]

To understand the slow homogenization (Figure 1) of melts, we used the Vogel−Fulcher−Tammann (VFT) variation of melt dynamics to estimate the melt viscosity at the reaction temperature. The shear relaxation time τ (T) variation in the VFT formalism can be written[60] in terms of melt fragility index m as follows,

$$\langle \tau \rangle = \tau_{VF} \exp[B/(T - T_0)] \tag{6}$$

where B is a fitting parameter and T_0 is a characteristic temperature less than T_g. The VFT formalism can then be related to melt fragility, m, by eq 7

$$\log\langle \tau \rangle = \log\langle \tau_g \rangle - m_{min} + m_{min}^2 (T_g/T) / [m - (m - m_{min})T_g/T] \tag{7}$$

Here T_g is identified with the temperature at which the relaxation time equals a characteristic value, usually taken to be $\tau(T_g) = \tau_g = 100$ s and m_{min} represents the lower limit of fragility taken[60] to be ~16. From the measured fragility index $m(x)$, we thus calculated the expected variation of melt viscosity $\eta(x)$ at 950 °C, the temperature at which Ge and S were reacted.

We also considered an alternative approach due to Mauro, Yeu, Ellison, Gupta, and Allan to describing the log $\eta(T_g/T)$ variation in glass forming melts. In this MYEGA[61] approach, the relationship between melt viscosity and fragility index can be written as follows:

$$\log_{10} \eta(T) = \log_{10} \eta_\infty + (12 - \log_{10} \eta_\infty)(T_g/T) \times \exp\left[\left(\frac{m}{12 - \log_{10} \eta_\infty}\right)\left(\frac{T_g}{T} - 1\right)\right] \tag{8}$$

where η_∞ represents the infinite temperature viscosity, usually taken as $\log_{10}\eta_\infty = -4$ at $m = 60$. Using the measured m, we have calculated η using eq 8. The diffusion coefficient, D, was estimated from the Eyring[62] relation (eq 9). In eq 9, parameter λ, represents the jump distance for viscous flow and is usually taken as a characteristic bond length of the network. From D, we estimated the characteristic diffusion length $L(x)$ using the Einstein relation (eq 10).

$$D = \frac{k_B T}{\eta \lambda} \tag{9}$$

$$L^2 = D \times t/6 \tag{10}$$

where t is the time of reaction.

Taking $\lambda = 2.05$ A° (typical jump distance, S−S bond distance), the results of our calculations of viscosity $\eta(x)$ and diffusion length $L(x)$ after $t = 1$ day for the MYEGA approach are plotted in Figure 12a. The VFT approach and the MYEGA approach for the present Ge−S binary melts reacted at 950 °C,

dx.doi.org/10.1021/jp411823j | J. Phys. Chem. B 2014, 118, 2249−2263

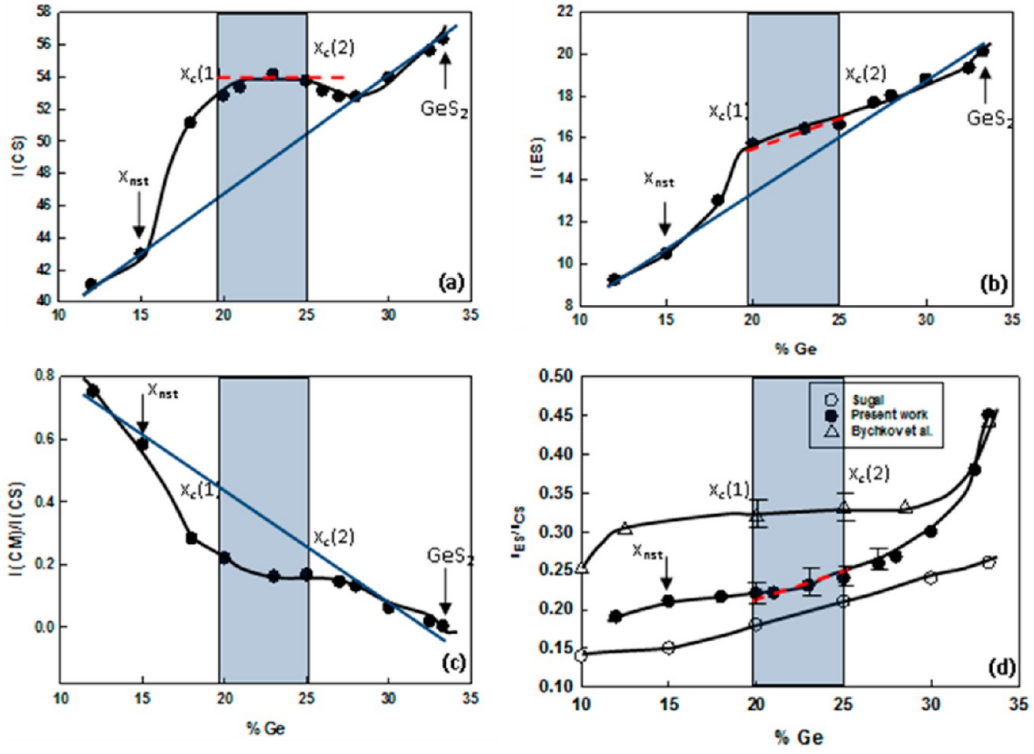

Figure 13. Variations in integrated scattering strength (I) of Raman modes of (a) A_1 mode of CS tetrahedra and (b) A_1^c edge sharing tetrahedral units. Scattering strength ratio of (c) S_n chain mode to CS mode and (d) A_1^c mode to A_1 mode from the present work (●), from Bychkov et al.[31] (Δ) and from Sugai[34] (○). Note that the scattering strength of modes in (a) and (b) and scattering strength ratios in (c) and (d) show a plateau-like behavior in the IP, which is suggestive of network adaption in that special phase.

yielded variations in viscosity $\eta(x)$ and diffusion length $L(x)$ (Figure 12a) that were almost identical.

We find (Figure 12a) that, for the superstrong melt composition near x = 25%, η displays a global maximum of $\sim 10^5$ Pa·s and leads to a global minimum of $L \sim 0.01$ mm. While these calculated values may not be exact, they are of the right order of magnitude. Given that the length of Ge−S melt column for the 1.5 g batch compositions used was about 20 mm, it is not surprising that reaction times of typically 3 weeks are needed to homogenize batch compositions (Figure 1). Thus, the homogenization kinetics of the nonstoichiometric Ge−S melts appear, in fact, to be limited by the slowest diffusing IP species,[40] that is, a superstrong composition near x = 25% of Ge.

4.3. Adaptation, Aging of Molar Volumes, Non-reversing Enthalpy of Relaxation, and Decoupling of S_8 Rings. One of the challenges in examining aging related effects in Ge−S glasses is that S-rich compositions (x < 25%) contain increasing fraction of S_8 rings (Figure 9 inset), and that the S_8 ring-fraction steadily increases upon aging of glasses over a period of weeks, as documented in Raman scattering results at x = 15% (Figure 11). Formation of S_8 rings at the expense of polymeric S_n chains is energetically favored. On the other hand, the reverse is the case for Se_8 rings and polymeric Se_n chains, and for that reason, one does not observe[39] such striking aging related decoupling of Se_8 rings in corresponding Ge−Se glasses.

Our results on molar volumes (Figure 10) and the enthalpy of relaxation at T_g, $\Delta H_{nr}(x)$ (Figure 12c) as a function of aging clearly show features that can be identified with the decoupling of S_8 rings from the backbone upon aging. The trapezoidal-like molar volume window $V_m(x)$ in Ge−S (Figure 10) deserves some comments. We have already noted that the V_m reduction for IP compositions is remarkably greater than for compositions outside the IP. Long range forces such as van der Waals and Coulomb assist network compaction. One might ask, why is the compaction effect so pronounced for IP compositions? This is the case because glassy networks in the IP are optimally constrained, that is, count of mechanical constraints due to short-range covalent forces (bond-stretching and bond-bending) is exactly 3, which leads to the formation of stress-free networks. And as glass backbones relax, long-range forces serve to compact IP networks as they adapt. Notice in the IP, the $\Delta H_{nr}(x)$ term ages minimally. On the other hand, stressed networks or flexible networks formed outside the IP compositions age and behave quite differently. Thus, we can understand the evolution of a volumetric window to be the signature of adaptation of the stress-free networks prevailing in that special elastic phase.

As a final comment, we note that the density of the stoichiometric GeS_2 glass reported by Zeidler et al.[37] of 2.72 g/cm^3 translates into a V_m of 16.75 cm^3. That value falls close to the one observed for our stoichiometric glass 6 weeks (16.7 cm^3) of aging. Molar volumes of the nonstoichiometric glasses have been reported by several groups[63] and were also summarized by Takabe et al.[30] A perusal of these results show wide variations as a function of composition, which we believe to be a reflection of glass heterogeneity. The results of Takebe et al.[30] are an exception, however. They also observe evidence of a global minimum of molar volumes in the IP window, which is similar to the trapezoidal window observed by us in the present work.

The aging of glass compositions as manifested by the $\Delta H_{nr}(x)$ term (Figure 12c) is most revealing and deserves some comments. At the outset, we recognize that in flexible and

dx.doi.org/10.1021/jp411823j | J. Phys. Chem. B 2014, 118, 2249−2263

stressed-rigid glass compositions, which are stressed,[17] the $\Delta H_{nr}(x)$ term, in general, is found to increase with waiting time. In sharp contrast, for IP glass compositions aging of the $\Delta H_{nr}(x)$ term is qualitatively suppressed because of the stress-free nature of the backbones.[17] Indeed, the near absence of the $\Delta H_{nr}(x)$ term in the IP is due the network reconnecting to expel stress-creating redundant bonds, that is, due to the network adapting. The sharpening of the upper edge of the reversibility window near x = 25% conforms to that expected behavior. But what are we to make of the lower edge of the reversibility window near x = 20% that shows the reverse behavior? We submit that the effect is a direct consequence of the S_8 rings decoupling. The aging-induced lowering of the $\Delta H_{nr}(x)$ term at x = 18% is due to the network backbone of this S-rich glass composition becoming somewhat Ge-richer due to the decoupling of S_8 rings from the backbone, rendering it closer to becoming optimally constrained, that is, $n_c \rightarrow 3$. These considerations lead naturally to a broadening of the lower end of the reversibility window wall due to decoupling of S_8 rings from the backbone.

4.4. Evolution of Ge_xS_{100-x} Glass Structure and the Nature of Chemical Order in the Stoichiometric GeS_2 Glass. The molecular structure evolution of Ge−S glasses has been elucidated by infrared reflectance,[29] Raman scattering,[34] and neutron scattering.[37,31] In the present Raman scattering measurements, we made a special effort to establish variations in mode scattering strengths with composition for the CS, ES, and chain modes, separately. The feature was made possible by the special procedure used for sample handling and data acquisition (section 2.3), and led, for the first time to the best of our knowledge, to observe a qualitative arrest of glass structure in the IP (Figure 13), as we describe below.

Elemental sulfur at ambient temperature possesses an orthorhombic structure[64,65] composed of S_8 rings. Upon heating, it transforms to a monoclinic form at 95.6 °C, and at still higher temperatures, exceeding 159 °C, into a highly viscous form (T_λ transition) composed of polymeric S_n chains. The Raman spectrum of elemental S as a function of T is well characterized.[66] Melt-quenched S-rich alloys consists of some glassy Ge−S backbone but with substantial amount of S present as S_8 rings. For example, at x = 12%, as revealed by Raman data (Figure 4) polymeric S_n chains cross-linked by Ge have evolved (Raman mode 460 cm^{-1}) with S_8 rings (modes at 147, 217, and 471 cm^{-1}) decoupling from that backbone. At these low Ge concentrations, the backbone (or connective tissue) of the NSPS network evolves stochastically, as evidenced by the observed variation of scattering strength of CS ($I_{CS}(x)$) and edge-sharing ($I_{ES}(x)$) tetrahedral units, and sulfur chain modes ($I_{CM}(x)$) with increasing x (Figure.13). The stochastic variation of scattering strengths then appears to be interrupted near $x = x_{nst}$ = 15%, as $I_{CS}(x)$, $I_{ES}(x)$, and $I_{CM}(x)$ vary nonlinearly with x. At $x < x_{nst}$, the backbone structure consists of weakly cross-linked S-chain network largely quasi 1D and evolves stochastically, as we will show below (Figure 14). But near x = 15%, GeS_4 chains emerge and the network morphology now increases to 2D or possibly 3D. The entanglement of the two chain structures not only slows the melt homogenization (Figure 12b) as the fragility index drops, the S_8 fraction decreases qualitatively as glasses become isostatically rigid and as x increases near to $x_c(1)$ = 20%, the rigidity transition.

In the 20% < x < 25% range, the scattering strength variation becomes rather exceptional, and one observes a plateau-like variation for the CS, ES, and S_n chain mode. The arrest in the

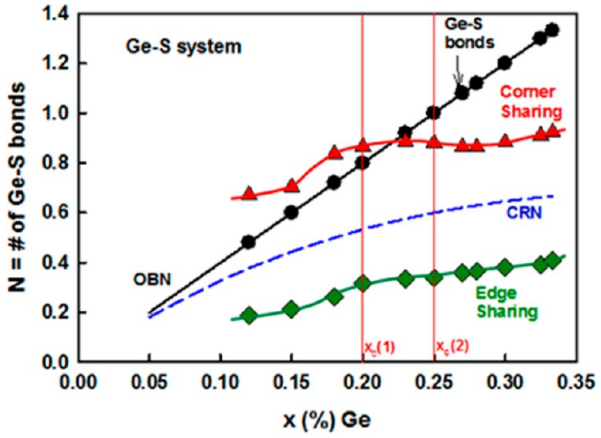

Figure 14. Variation in the concentration of Ge−S bonds, $N(x) = I_n/\sigma_n$ (●), coming from CS tetrahedral units $N_{CS}(x)$ ((▲), and from ES tetrahedral units $N_{ES}(x)$ (♦) in Ge_xS_{100-x} glasses deduced from Raman scattering. The concentrations $N(x)$ were obtained by adding together I_{CS}/σ_{CS} with I_{ES}/σ_{ES} and normalizing the sum to a value of 4/3 at x = 0.33. The linear $N(x)$ variation conforms well to the ordered bond network (OBN) prediction, but not the CRN one. The $N_{CS}(x)$ and $N_{ES}(x)$ could be uniquely determined by their ratio at x = 1/3 from the measured intensity ratio and Raman cross sections (σ_n). No corrections for the segregated S_8 fraction were made for the low Ge content (x < 25%) glasses.

scattering strengths of the CS and ES tetrahedral units even when the backbone cross-link density is steadily increasing (as T_g continues to increase (Figure 8a)) is evidence of the network adapting to expel attendant stress by reconnecting. The nonreversing enthalpy (Figure 8b) continues to remain minuscule in that range, which is strong evidence of isostaticity of the network.[19] Thus, the appearance of a reversibility window, a volumetric window, a fragility minimum, and with the Raman optical elastic power-law behavior of p = 1 for CS mode confirms the truly exceptional physical behavior of glasses in the intermediate phase.

The observation of the nonreversing enthalpy $\Delta H_{nr}(x)$ abruptly increasing (Figure 12c) by an order of magnitude as x > 25%, is in harmony with the onset of a percolative stress transition.[14] At x > 25%, the ES mode scattering strength grows almost linearly (Figure 13b), signaling that backbone is now overconstrained and in the stressed-rigid elastic phase. Confirmation is given by the optical elasticity variation of the CS mode frequency squared with composition that displays characteristic power-law, p = 1.32 (Table 1), in harmony with numerical simulations.[53,54]

And as one approaches the stoichiometric composition, x = 33.3%, a NSPS transition occurs near 31%, where Ge−Ge bonds first form and decouple from the backbone. The maximum in the slope dT_g/dx (Figure 8a) at this composition suggests a change in network topology; glass compositions at x > 31% are segregated into S-rich and Ge-rich phases leading thereafter to the stoichiometric glass GeS_2[12,67] to be mildly segregated.[35,68] In the stoichiometric glass we can detect the vibrational mode of the ethane-like units.[46,47] From the measured scattering strength ratio of the ethane-like mode near 260 cm^{-1} to the CS mode near 340 cm^{-1}, normalized with respect to their Raman cross sections, we obtain the fraction of ethane-like units to CS units at 0.78%.[43] Given that for GeS_2 glass, there are 0.43 ES units for each CS unit (Figure 13), and in each of these we have 4 Ge−S bonds, we deduce the fraction

dx.doi.org/10.1021/jp411823j | J. Phys. Chem. B 2014, 118, 2249−2263

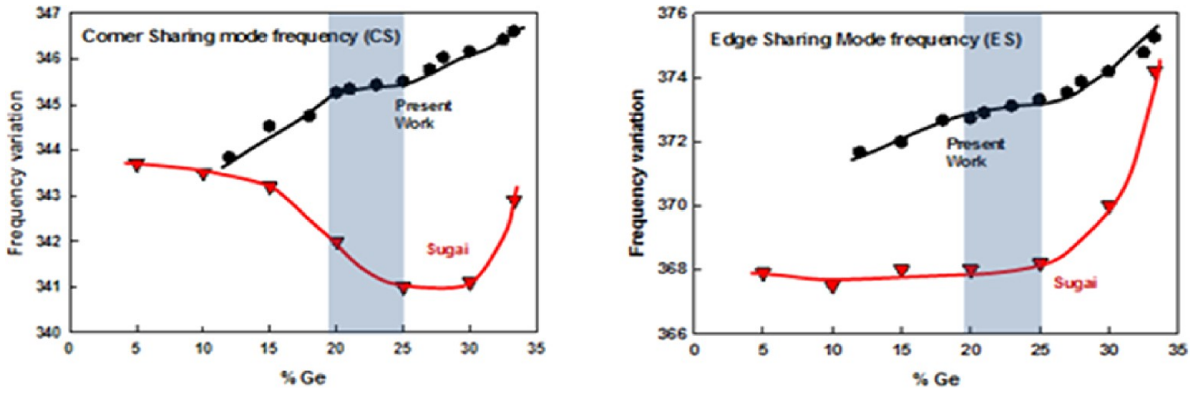

Figure 15. Variations in Raman frequency of (a) A_1 mode of corner-sharing GeS_4 and (b) A_1^C Raman mode of edge-sharing tetrahedral from the present work (●) and the work of Sugai (▼) ref [34]. The data points from Sugai's work are taken from Table 2 of ref 34. In the present work, the mode frequency squared was used to extract elastic power laws in the intermediate phase (blue panel) and the stressed-rigid phase ($x > 25\%$). See Figure 5.

of N_{Ge-Ge}/N_{Ge-S} bonds to be 0.14(5)%. Our present estimate of homopolar bonds in the more homogeneous GeS_2 glass is smaller than our earlier estimate of 1.2%.[35]

The molecular structure of GeS_2 glass has been examined in neutron structure factor measurements,[31,37] and these results have been analyzed in first principles MD simulations.[47,69,70] In the most recent contribution, Celino et al.[67] point out that of the 4-fold Ge and 2-fold S present in GeS_2, a substantial fraction (Table 3 in ref 67) occur as homopolar (Ge−Ge, 10%) and S−S (16%) bonds. These estimates are higher than the present experimental results and suggest that the difficulty of slow cooling melts close to T_g in MD simulations continues to be a challenge. However, it is interesting to note that the simulations reveal homopolar S−S bonds to largely come from S atoms having a Ge and a S nearest neighbor, a local coordination that would result naturally from the outrigger S−S bonds[71] formed in the high-T phase of c-GeS_2. The ES/CS fraction of this moiety is 0.5, close to the fraction of 0.43(4) reported from the two neutron scattering[31,37] reports and present Raman scattering data. It was again the presence of the outrigger S−S bonds in GeS_2 glass that led the oversized ^{129m}Te parent to selectively replace the chemically disordered outrigger S sites in the stoichiometric glass to account for the observed ^{129}I Mossbauer spectrum.[72]

Two types of model descriptions of binary $Ge_x(S \text{ or } Se)_{100-x}$ networks have gained popularity, a continuous random network (CRN)[34] and an ordered bond network (OBN) or chain-crossing model,[29] where the local structure of Ge is 4-fold coordinated to S atoms, as in the GeS_2. In the former case (CRN), Ge−Ge, S−S, and Ge−S bonds are formed randomly based on atom concentrations, and the predicted[29] variation of Ge−S bond concentration $N(x)$ is given as

$$N_{CRN} = 4x(1 - x)/[1 + x] \quad (11)$$

In an OBN model, bond energies are a weighting factor, in addition, and lead the Ge−S bond concentration $N(x)$ to vary[29] as

$$N_{OBN} = 4x \quad (12)$$

Thus, at $x = 0$, only S−S bonds exist, while at $x = 1/3$, only Ge−S bonds exist in an OBN, with the count of these bonds equal to $N = 4x = 4/3$.

The concentration of Ge−S bonds in glasses was deduced from present Raman scattering as follows. The working assumption is that the Raman integrated intensity (I_n) is determined by the concentration (N_n) of the species, the scattering cross-section (σ_n) and other factors (G_n) that include the exciting laser power density and geometrical factors such as planarity of glass surface and light collection optics.

$$I_n = N_n \sigma_n G_n \quad (13)$$

The factor G was specially controlled (section 2.2) in the compositional studies as mentioned earlier and remained independent of x. The cluster calculations[46] place the cross-section of CS tetrahedral and ES tetrahedral units at 77.5 and 79.5 A^4/esu, respectively. The sum of the concentrations $N_{CS} + N_{ES}$ was then normalized at $x = 1/3$ to 4/3 following eq 12 (see Figure 14). The observed variation of the count of Ge−S bonds show a linear behavior with x, results that are in harmony with an earlier IR measurement.[29] In the IR reflectance experiments, one examined[29] the F_2 active vibrational mode strength (of GeS_4 tetrahedra near 367 cm^{-1}) by obtaining the imaginary part (ε_2) of the dielectric function. Furthermore, the OBN description is also consistent with the higher Pauling single bond strength of Ge−S bonds (55.52 kcal/mol)[73] than of Ge−Ge bonds (37.6 kcal/mol) and S−S bonds (50.9 kcal/mol), thus, promoting growth of heteropolar bonds at the expense of homopolar ones.

4.5. Variance in the Reported Physical Properties of Nonstoichiometric Ge−S Melts and Glasses: The Influence of Compositional Heterogeneity. Bulk glasses of the stoichiometric GeS_2 composition homogenize more easily than nonstoichiometric compositions because of the underlying crystalline phases that promote growth of chemical order. Thus, the data of Figure 7 broadly shows that the spread in T_g of the stoichiometric glass between various reports of 30 °C (from a low value of 495 °C to a high value of 525 °C) is actually quite small compared to the variation encountered for nonstoichiometric compositions. Since the $T_g(x)$ variation in Ge−S glasses maximizes near the stoichiometric composition, it follows that glasses with a T_g lower than the maximum value of 518 °C (Figure 7) possess a larger spread in Ge stoichiometry variation, "Δx" across a sample, that is, are more heterogeneous.

Nonstoichiometric chalcogenides melts/glasses[9,13,40] undergo slow homogenization, as we noted earlier, because of the superstrong character of melt compositions in the IP (section 4.2.2). Not surprisingly, reports of T_g of the $Ge_{25}S_{75}$ glass

dx.doi.org/10.1021/jp411823j | J. Phys. Chem. B 2014, 118, 2249−2263

composition show a wide variation; 139 °C on the low side,[63] to values of 340 °C in ref 31, 360 °C in ref 33, and 370 °C in the present work. The spread of T_g between the high and the low value is now 230 °C for this nonstoichiometric composition and stands in sharp contrast to the rather narrow spread noticed earlier for the stoichiometric composition GeS_2 (Figure 7). The large spread in T_g is a direct reflection of glass heterogeneity.

The molecular structure of binary Ge−S glasses has been discussed in several earlier reports[29−32,34,45,74,75] and we now compare these with the present findings. Sugai[34,76] reported on dispersive Raman scattering on Ge−S glasses and suggested that the structure of these glasses is best described as a CRN. Regrettably, we could not find details of glass synthesis or calorimetric characterization of the glass samples used by Sugai. However, we can directly compare the compositional variation in the CS and ES mode frequencies reported by Sugai with the present work (Figure 15). The red-shift of the CS mode with increasing x at $x > 15\%$ and the near constancy of the ES mode frequency in the $5\% < x < 25\%$ range of composition reported by Sugai is qualitatively at odds with the present results on glasses of proven homogeneity. In our experiments, the elastic power-laws for both the ν_{CS}^2 and ν_{ES}^2 in the IP and the stressed-rigid phase were inferred from a blue-shift of these modes with x, as also in earlier reports on the Ge−Se[9] and Si−Se[3] binary systems. Indeed, increased cross-linking with increasing x will fundamentally stiffen the network and lead CS and ES modes to blue-shift. Thus, the mode frequency variation reported by Sugai is also physically unrealistic. These differences are due to sample make up and cast serious doubts on the validity of a strictly CRN description of the present glasses across the wide range of Ge concentration. It is highly likely that, in heterogeneous Ge−S glasses for which a CRN description is favored,[34] the intermediate phase will not exist. Indeed, a parallel circumstance has recently been noted in the Ge−Se glasses.[77]

For the stoichiometric composition, the ES/CS fraction found by Bychkov et al.[31] of 0.44(3) and by Zeidler et al.[37] of 0.47(5), both from neutron scattering, are in excellent agreement with the present Raman result yielding a value of 0.43(2). Raman scattering measurements are subject to matrix element effects. An estimate of the Raman cross-section of ES and CS modes from cluster calculations[46] place $\sigma_{ES} = 79.3$ A^4/esu and $\sigma_{CS} = 77.5$ A^4/esu. Correcting the observed Raman scattering strength ratio of ES/CS modes of 0.44(2), for the Raman cross sections, we deduce an ES/CS fraction of 0.43(2) from the present Raman measurements.

On the other hand, a qualitatively different picture emerges for nonstoichiometric compositions, where clear disagreements appear between the present Raman and the earlier neutron scattering results of Bychkov et al.[31] For example, at $Ge_{25}S_{75}$, the neutron scattering results place the ES/CS ratio at 0.32(3), higher than the present Raman ES/CS fraction of 0.22(2).

The compositional width of the IP found in the present Ge−S glasses almost coincides (Table1) with the one in Ge−Se glasses.[9,10,13] There is an intimate and deep connection between glass structure and the IP width that was first recognized by Micoulaut and Phillips[6] based on cluster expansion calculations (size increasing cluster agglomeration, SICA). Specifically, they demonstrated that in these IV−VI glasses the ES/CS fraction controls the width of the IP, an idea for which significant support has emerged since.[52] The close similarity of ES/CS fraction in Ge−S and Ge−Se glasses deduced from Raman scattering is quite consistent with the IP width being nearly the same.[43] On the other hand, the higher ES/CS fraction obtained by Bychkov et al.[31] would require the IP width in Ge−S glasses to exceed the one in Ge−Se glasses.

Bychkov et al.[31] synthesized their samples by reaction of the starting materials in the 700 to 1100 °C range for a period up to 120 h (~5 days), in sharp contrast to almost 21 days needed to homogenize 1.5 g sized batches in the present Raman profiling experiments. Here it is important to emphasize that the kinetics of melt homogenization at nonstoichiometric composition is limited by the slowest diffusing[40] intermediate phase species, that is, the superstrong composition near $x = 25\%$ (Figure 10). Thus, the lack of reproducibility of the ES/CS fraction for nonstoichiometric compositions, in our view, derives from the makeup of samples, an issue that needs to be seriously considered in future studies.

Malek et al.[49] synthesized Ge_xS_{100-x} glasses at $x = 30\%$, 32%, 33% and 33.3% and examined T_g and fragility from viscosity measurements. For a glass composition at $x = 30\%$, they observed a $T_g = 362$ °C, which may be compared to a $T_g = 429$ °C in the present work. The fragility index for such a sample was reported at 30(2) compared to a value of 23(2), which we observed from AC calorimetric measurements. A similar pattern is observed at other compositions. The consistently lower T_g and higher m obtained by Malek et al.[49] compared to the present data may be suggestive that the glass samples used in the viscosity measurements were probably not as homogeneous as the present ones. The suggestion is consistent with the synthesis conditions employed by Malek et al.,[49] who reacted the starting materials at 900 °C for only 12 h. Under those conditions of synthesis, a melt at $x = 30\%$ (Figure 1), our Raman profiling data reveals a glass to be rather heterogeneous. These conclusions are actually similar to those observed in Ge−Se[9] and As−Se[55] melts. Fragilities of inhomogeneous melts are found to be upshifted with respect to those of homogeneous ones.

Molar volumes provide valuable information on network packing of glasses and are deeply influenced by their homogeneity.[9,55,77] We have already noted that the trapezoidal window in V_m centered in the $15\% < x < 25\%$ range observed by us and separately by Takebe et al.[30] are quite similar (Figure 10). However, reports from several other groups do not show the same behavior; for example, Saffarini[63] found a sharply defined narrow minimum at $x = 22\%$ (15.86 cm^3); on the other hand, Zhilinskaya et al.[78] observed just the opposite behavior, a maximum in $V_m(x)$ near $x = 23\%$ (16.9 cm^3). These large variations in $V_m(x)$ of these nonstoichiometric compositions, once again, are signatures of glass heterogeneity by virtue of synthesis.[77]

In summary, perusal of the published data on Ge−S glasses synthesized by reaction of the starting materials of several gram batches at a suitable high temperature (700−950 °C) for several tens of hours appear to be heterogeneous. The large spread in physical properties such as T_g, fragility index, ES/CS ratio, and $V_m(x)$ from one group to the other far exceeding the errors of measurement is a direct reflection of glass heterogeneity. The slow homogenization of nonstoichiometric chalcogenides melts/glasses is an impediment in developing reliable structural models of these fascinating materials because of nonreproducibility of the available data. It is crucial that variance of molar volumes and calorimetric T_gs across batch compositions be ascertained[77] as a test of glass homogeneity

dx.doi.org/10.1021/jp411823j | J. Phys. Chem. B 2014, 118, 2249−2263

before undertaking more exotic measurements to build structural models of glasses.

5. CONCLUSIONS

Calorimetric, volumetric, and Raman scattering measurements of specially homogenized Ge_xS_{100-x} melts/glasses show at low x, 12% < x < 20%, to be in the flexible phase, and in the 19.3(5)% < x < 24.9(5)% range to self-organize and display an intermediate phase (IP). At higher x, in the 24.9(5)% < x < 33.3(5)% range, networks become stressed-rigid. These transitions are accurately fixed by Raman scattering in which the CS and ES mode frequency displays a blue-shift with x and kinks at the two elastic thresholds (rigidity, 19.3(5)%, and stress, 24.9(5)%), and the underlying optical elasticity display power laws in both the IP and the stressed-rigid phase. The reversibility window from calorimetric measurements displays a nearly square-well like behavior with window walls coinciding with the rigidity and stress transitions. In the IP the scattering strength of CS GeS_4 mode become nearly independent of x even though the Ge content continues to increase linearly, an observation that constitute evidence of network adaptation. Molar volumes in aged glasses reveal a volumetric window with walls that coincide with the reversibility window. Complex C_p measurements show fragility index, $m(x)$, to show a global minimum that correlates with the reversibility window, the former characteristic of melts ($T > T_g$) while the latter of glasses ($T < T_g$). The strong nature of melts in the IP leads to slow kinetics of melt-homogenization. Elastic phases in the present Ge_xS_{100-x} binary, in conjunction with the ones reported earlier in As_xS_{100-x} binary,[79] and in the $Ge_xAs_xS_{100-2x}$ ternary[80] has permitted establishing the global elastic phase diagram of the Ge−As−S ternary (TOC). Appearance of the flexible, isostatically rigid IP, and the stressed-rigid elastic phase in the present sulfides as in other selenide glasses is strong validation that onset of rigidity driven by network topology provides a sound basis to understanding the compositional variation in physical and chemical properties of network glasses.

AUTHOR INFORMATION

Corresponding Author

*Phone: 513-556-4790. E-mail: boolchp@ucmail.uc.edu.

Funding

This work was supported by NSF Grant DMR-08-53957.

Notes

The authors declare no competing financial interest.

ACKNOWLEDGMENTS

We have benefited from useful discussions with Dr. M. Micoulaut, Dr. J. C. Phillips, and Dr. S. Mamedov during the course of this work. Discussions and assistance from Dr. W. J. Bresser and S. Hall in calorimetric studies is acknowledged with pleasure.

REFERENCES

(1) Phillips, J. C. Topology of Covalent Non-Crystalline Solids I: Short-Range Order in Chalcogenide Alloys. *J. Non-Cryst. Solids* **1979**, *34*, 153−181.

(2) Thorpe, M. F. Continuous Deformations in Random Networks. *J. Non-Cryst. Solids* **1983**, *57*, 355−370.

(3) Selvanathan, D.; Bresser, W.; Boolchand, P. Stiffness Transitions in Si_x Se_{1-x} Glasses from Raman Scattering and Temperature-Modulated Differential Scanning Calorimetry. *Phys. Rev. B* **2000**, *61*, 15061.

(4) Selvanathan, D.; Bresser, W.; Boolchand, P.; Goodman, B. Thermally Reversing Window and Stiffness Transitions in Chalcogenide Glasses. *Solid State Commun.* **1999**, *111*, 619−624.

(5) Thorpe, M.; Jacobs, D.; Chubynsky, M.; Phillips, J. Self-Organization in Network Glasses. *J. Non-Cryst. Solids* **2000**, *266*, 859−866.

(6) Micoulaut, M.; Phillips, J. C. Rings and Rigidity Transitions in Network Glasses. *Phys. Rev. B* **2003**, *67*, 104204.

(7) Micoulaut, M.; Kachmar, A.; Bauchy, M.; Le Roux, S.; Massobrio, C.; Boero, M. Structure, Topology, Rings, and Vibrational and Electronic Properties of Ge_x Se_{1-x} Glasses across the Rigidity Transition: A Numerical Study. *Phys. Rev. B* **2013**, *88*, 054203.

(8) Boolchand, P.; Feng, X.; Bresser, W. Rigidity Transitions in Binary Ge−Se Glasses and the Intermediate Phase. *J. Non-Cryst. Solids* **2001**, *293*, 348−356.

(9) Bhosle, S.; Gunasekera, K.; Boolchand, P.; Micoulaut, M. Melt Homogenization and Self-Organization in Chalcogenides: Part II. *Int. J. Appl. Glass Sci.* **2012**, *3*, 205−220.

(10) Bhosle, S.; Gunasekera, K.; Chen, P.; Boolchand, P.; Micoulaut, M.; Massobrio, C. Meeting Experimental Challenges to Physics of Network Glasses: Assessing the Role of Sample Homogeneity. *Solid State Commun.* **2011**, *151*, 1851−1855.

(11) Salmon, P. S.; Petri, I. Structure of Glassy and Liquid Ge Se_2. *J. Phys. Cond. Matter* **2003**, *15*, S1509.

(12) Boolchand, P.; Bresser, W. The Structural Origin of Broken Chemical Order in $GeSe_2$ Glass. *Philos. Mag. B* **2000**, *80*, 1757−1772.

(13) Bhosle, S.; Gunasekera, K.; Boolchand, P.; Micoulaut, M. Melt Homogenization and Self-Organization in Chalcogenides: Part I. *Int. J. Appl. Glass Sci.* **2012**, *3*, 189−204.

(14) Chubynsky, M. V.; Thorpe, M. F. The Intermediate Phase and Self-Organization in Network Glasses. In *Phase Transitions and Self-Organization in Electronic and Molecular Networks*; Phillips, J. C., Thorpe, M. F., Eds.; Kluwer Academic/Plenum Publishers: New York, 2001; p 4364.

(15) Chubynsky, M. V. Characterizing Intermediate Phases through Topological Analysis. In *Rigidity and Boolchand Intermediate Phases in Nanomaterials*; Micoulaut, M., Popescu, M., Eds.; INOE Publishing House: U.K., 2009; pp 213−226.

(16) Boolchand, P.; Georgiev, D.; Goodman, B. Discovery of the Intermediate Phase in Chalcogenide Glasses. *J. Opt. Adv. Mater.* **2001**, *3*, 703−720.

(17) Wang, F.; Mamedov, S.; Boolchand, P.; Goodman, B.; Chandrasekhar, M. Pressure Raman Effects and Internal Stress in Network Glasses. *Phys. Rev. B* **2005**, *71*, 174201.

(18) Boolchand, P. Insulating and Semiconducting Glasses. In *Insulating And Semiconducting Glasses. Series on Directions in Condensed Matter Physics*; Boolchand, P., Ed.; World Scientific: Singapore, 2000; vol. *17*, 978−981−02−3673−1.

(19) Micoulaut, M. Linking Rigidity Transitions with Enthalpic Changes at the Glass Transition and Fragility: Insight from a Simple Oscillator Model. *J. Phys. Cond. Matter* **2010**, *22*, 285101.

(20) Guo, X.; Mauro, J. C.; Allan, D. C.; Yue, Y. On the Frequency Correction in Temperature-Modulated Differential Scanning Calorimetry of the Glass Transition. *J. Non-Cryst. Solids* **2012**, *358*, 1710−1715.

(21) Boolchand, P.; Chen, P.; Novita, D.; Goodman, B. New Perspectives on Intermediate Phases. *Rigidity and Boolchand Intermediate Phases in Nanomaterials*; INOE Publishing House: Romania, 2009; pp 1−36.

(22) Barre, J.; Bishop, A. R.; Lookman, T.; Saxena, A. Adaptability and "Intermediate Phase" in Randomly Connected Networks. *Phys. Rev. Lett.* **2005**, *94*, 208701−4.

(23) Brière, M.-A.; Chubynsky, M.; Mousseau, N. Self-Organized Criticality in the Intermediate Phase of Rigidity Percolation. *Phys. Rev. E* **2007**, *75*, 056108.

(24) Chubynsky, M.; Briere, M.-A.; Mousseau, N. Self-Organization with Equilibration: A Model for the Intermediate Phase in Rigidity Percolation. *Phys. Rev. E* **2006**, *74*, 016116.

(25) Vaills, Y.; Qu, T.; Micoulaut, M.; Chaimbault, F.; Boolchand, P. Direct Evidence of Rigidity Loss and Self-Organization in Silicate Glasses. *J. Phys. Cond. Matter* **2005**, *17*, 4889.
(26) Chakraborty, S.; Boolchand, P.; Malki, M.; Micoulaut, M. Designing Heavy Metal Oxide Glasses with Threshold Properties from Network Rigidity. *J. Chem. Phys.* **2013**, *140*, 014503.
(27) Novita, D. I.; Boolchand, P.; Malki, M.; Micoulaut, M. Fast-Ion Conduction and Flexibility of Glassy Networks. *Phys. Rev. Lett.* **2007**, *98*, 195501.
(28) Micoulaut, M.; Malki, M. Direct Evidence of a Characteristic Length Scale of a Dynamical Nature in the Boolchand Phase of Glasses. *Phys. Rev. Lett.* **2010**, *105*, 235504.
(29) Lucovsky, G.; Galeener, F. L.; Keezer, R. C.; Geils, R.; Six, H. Structural Interpretation of the Infrared and Raman Spectra of Glasses in the Alloy System $Ge_{1-x}S_x$. *Phys. Rev. B* **1974**, *10*, 5134.
(30) Takebe, H.; Maeda, H.; Morinaga, K. Compositional Variation in the Structure of Ge−S Glasses. *J. Non-Cryst. Solids* **2001**, *291*, 14−24.
(31) Bychkov, E.; Miloshova, M.; Price, D.; Benmore, C.; Lorriaux, A. Short, Intermediate and Mesoscopic Range Order in Sulfur-Rich Binary Glasses. *J. Non-Cryst. Solids* **2006**, *352*, 63−70.
(32) Kawamoto, Y.; Tsuchihashi, S. Properties and Structure of Glasses in the System Ge−S. *J. Am. Ceram. Soc.* **1971**, *54*, 131−135.
(33) Feng, X.; Bresser, W.; Boolchand, P. Direct Evidence for Stiffness Threshold in Chalcogenide Glasses. *Phys. Rev. Lett.* **1997**, *78*, 4422.
(34) Sugai, S. Stochastic Random Network Model in Ge and Si Chalcogenide Glasses. *Phys. Rev. B* **1987**, *35*, 1345.
(35) Cai, L.; Boolchand, P. Nanoscale Phase Separation of GeS_2 Glass. *Philos. Mag. B* **2002**, *82*, 1649−1657.
(36) Boolchand, P.; Gunasekera, K.; Bhosle, S. Midgap States, Raman Scattering, Glass Homogeneity, Percolative Rigidity and Stress Transitions in Chalcogenides. *Phys. Status Solidi* **2012**, *249*, 2013−2018.
(37) Zeidler, A.; Drewitt, J. W.; Salmon, P. S.; Barnes, A. C.; Crichton, W. A.; Klotz, S.; Fischer, H. E.; Benmore, C. J.; Ramos, S.; Hannon, A. C. Establishing the Structure of GeS_2 at High Pressures and Temperatures: A Combined Approach Using X-ray and Neutron Diffraction. *J. Phys. Cond. Matter* **2009**, *21*, 474217.
(38) Murase, K.; Yakushiji, K.; Fukunaga, T. Interaction among Cluster in Chalcogen-Rich Glasses of Ge_{1-x} (S or Se)$_x$. *J. Non-Cryst. Solids* **1983**, *59*, 859−862.
(39) Chen, P.; Boolchand, P.; Georgiev, D. Long Term Aging of Selenide Glasses: Evidence of Sub-T_g Endotherms and Pre-T_g Exotherms. *J. Phys.: Condens. Matter* **2010**, *22*, 065104.
(40) Gunasekera, K.; Bhosle, S.; Boolchand, P.; Micoulaut, M. Superstrong Nature of Covalently Bonded Glass-Forming Liquids at Select Compositions. *J. Chem. Phys.* **2013**, *139*, 164511.
(41) Carpentier, L.; Desprez, S.; Descamps, M. From Strong to Fragile Glass-Forming Systems: A Temperature Modulated Differential Scanning Calorimetry Investigation. *Phase Transitions* **2003**, *76*, 787−799.
(42) Bustin, O.; Descamps, M. Slow Structural Relaxations of Glass-Forming Maltitol by Modulated DSC Calorimetry. *J. Chem. Phys.* **1999**, *110*, 10982.
(43) Chakraborty, S. Topological Origin of Glass Formation, Rigidity and Stress Transitions, Conductivity and Fragility in Specially Homogeneous Heavy Metal Oxide and Chalcogenide Systems. *Ph.D. Dissertation*, University of Cincinnati, Cincinnati, OH, 2014.
(44) Bhosle, S. V. Direct Evidence for Abrupt Rigidity and Stress Transitions in Dry and Homogeneous Bulk Ge_xSe_{100-x} Glasses. *M.S. Thesis*, University of Cincinnati, Cincinnati, OH, 2011.
(45) Kalampounias, A.; Andrikopoulos, K.; Yannopoulos, S. Probing the Sulfur Polymerization Transition in Situ with Raman Spectroscopy. *J. Chem. Phys.* **2003**, *118*, 8460.
(46) Jackson, K.; Briley, A.; Grossman, S.; Porezag, D. V.; Pederson, M. R. Raman-Active Modes of α-$GeSe_2$ and α-GeS_2: A First-Principles Study. *Phys. Rev. B* **1999**, *60*, R14985.
(47) Blaineau, S.; Jund, P. Vibrational Signature of Broken Chemical Order in a Ges_{2} Glass: A Molecular Dynamics Simulation. *Phys. Rev. B* **2004**, *69*, 064201.
(48) Manara, D.; Grandjean, A.; Neuville, D. Advances in Understanding the Structure of Borosilicate Glasses: A Raman Spectroscopy Study. *Am. Mineral.* **2009**, *94*, 777−784.
(49) Málek, J.; Shánělová, J. Viscosity of Germanium Sulfide Melts. *J. Non-Cryst. Solids* **1999**, *243*, 116−122.
(50) Micoulaut, M.; Naumis, G. Glass Transition Temperature Variation, Cross-Linking and Structure in Network Glasses: A Stochastic Approach. *Europhys. Lett.* **1999**, *47*, 568.
(51) Wang, L.-M.; Mauro, J. C. An Upper Limit to Kinetic Fragility in Glass-Forming Liquids. *J. Chem. Phys.* **2011**, *134*, 044522.
(52) Gunasekera, K.; Boolchand, P.; Micoulaut, M. Elastic Phases of Ge_x Sb_xSe_{100-2x} Ternary Glasses Driven by Topology. *J. Phys. Chem. B* **2013**, *117*, 10027−10034.
(53) He, H.; Thorpe, M. Elastic Properties of Glasses. *Phys. Rev. Lett.* **1985**, *54*, 2107.
(54) Franzblau, D.; Tersoff, J. Elastic Properties of a Network Model of Glasses. *Phys. Rev. Lett.* **1992**, *68*, 2172.
(55) Ravindren, S.; Gunasekera, K.; Tucker, Z.; Diebold, A.; Boolchand, P.; Micoulaut, M., Crucial Effect of Glass Processing and Melt Homogenization on the Fragility of Non-Stoichiometric Chalcogenides. *arXiv preprint* **2013**, DOI: arXiv:submit/0855094.
(56) Qin, Q.; McKenna, G. B. Correlation between Dynamic Fragility and Glass Transition Temperature for Different Classes of Glass Forming Liquids. *J. Non-Cryst. Solids* **2006**, *352*, 2977−2985.
(57) Williams, M. L.; Landel, R. F.; Ferry, J. D. The Temperature Dependence of Relaxation Mechanisms in Amorphous Polymers and Other Glass-Forming Liquids. *J. Am. Chem. Soc.* **1955**, *77*, 3701−3707.
(58) Angell, A. C. Relaxation in Liquids, Polymers and Plastic Crystals: Strong/Fragile Patterns and Problems. *J. Non-Cryst. Solids* **1991**, *131*, 13−31.
(59) Rault, J. Origin of the Vogel−Fulcher−Tammann Law in Glass-Forming Materials: The A−B Bifurcation. *J. Non-Cryst. Solids* **2000**, *271*, 177−217.
(60) Böhmer, R.; Ngai, K.; Angell, C.; Plazek, D. Nonexponential Relaxations in Strong and Fragile Glass Formers. *J. Chem. Phys.* **1993**, *99*, 4201.
(61) Mauro, J. C.; Yue, Y.; Ellison, A. J.; Gupta, P. K.; Allan, D. C. Viscosity of Glass-Forming Liquids. *Proc. Natl. Acad. Sci. U.S.A.* **2009**, *106*, 19780−19784.
(62) Bauchy, M.; Guillot, B.; Micoulaut, M.; Sator, N. Viscosity and Viscosity Anomalies of Model Silicates and Magmas: A Numerical Investigation. *Chem. Geol.* **2013**, *346*, 47−56.
(63) Saffarini, G. Glass Transition Temperature and Molar Volume Versus Average Coordination Number in $Ge_{100-x}S_x$ Bulk Glasses. *Appl. Phys. A: Mater. Sci. Process.* **1994**, *59*, 385−388.
(64) Warren, B.; Burwell, J. The Structure of Rhombic Sulphur. *J. Chem. Phys.* **1935**, *3*, 6.
(65) Abrahams, S. C. The Crystal and Molecular Structure of Orthorhombic Sulfur. *Acta Crystallogr.* **1955**, *8*, 661−671.
(66) Ward, A. T. Raman Spectroscopy of Sulfur, Sulfur−Selenium, and Sulfur−Arsenic Mixtures. *J. Phys. Chem.* **1968**, *72*, 4133−4139.
(67) Celino, M.; Le Roux, S.; Ori, G.; Coasne, B.; Bouzid, A.; Boero, M.; Massobrio, C. First-Principles Molecular Dynamics Study of Glassy GeS_2: Atomic Structure and Bonding Properties. *Phys. Rev. B* **2013**, *88*, 174201.
(68) Bresser, W.; Boolchand, P.; Suranyi, P. Rigidity Percolation and Molecular Clustering in Network Glasses. *Phys. Rev. Lett.* **1986**, *56*, 2493.
(69) Blaineau, S.; Le Roux, S.; Jund, P. Ab Initio Molecular Dynamics Study of GeS_2: From the Crystal to the Glass. *J. Phys.: Condens. Matter* **2007**, *19*, 455207.
(70) Blaineau, S.; Jund, P.; Drabold, D. A. Physical Properties of a GeS_2 Glass Using Approximate Ab Initio Molecular Dynamics. *Phys. Rev. B* **2003**, *67*, 094204.

(71) Bridenbaugh, P.; Espinosa, G.; Griffiths, J.; Phillips, J.; Remeika, J. Microscopic Origin of the Companion A_1 Raman Line in Glassy $Ge(S, Se)_2$. *Phys. Rev. B* **1979**, *20*, 4140.
(72) Bresser, W.; Boolchand, P.; Suranyi, P.; De Neufville, J. Direct Evidence for Intrinsically Broken Chemical Ordering in Melt-Quenched Glasses. *Phys. Rev. Lett.* **1981**, *46*, 1689.
(73) Pauling, L., *The Nature of the Chemical Bond and the Structure of Molecules and Crystals: An Introduction to Modern Structural Chemistry*; Cornell University Press: Ithaca, NY, 1960.
(74) Aitken, B. G.; Quimby, R. S. Rare-Earth-Doped Multi-component Ge-Based Sulphide Glasses. *J. Non-Cryst. Solids* **1997**, *213*, 281−287.
(75) Turnbull, D.; Aitken, B.; Bishop, S. Broad-Band Excitation Mechanism for Photoluminescence in Er-Doped $Ge_{25}Ga_{1.7}As_{8.3}S_{65}$ Glasses. *J. Non-Cryst. Solids* **1999**, *244*, 260−266.
(76) Sugai, S. Two-Directional Photoinduced Crystallization in $GeSe_2$ and $SiSe_2$ Glasses. *Phys. Rev. Lett.* **1986**, *57*, 456−459.
(77) Bhageria, R.; Gunasekera, K.; Boolchand*, P.; Micoulaut, M. Fragility and Molar Volumes of Non-Stoichiometric Chalcogenides: the Crucial Role of Melt/Glass Homogenization. *Phys. Status Solidi* **2014**, 1−9.
(78) Zhilinskaya, E.; Valeev, N. K.; Oblasov, A. Ge_xS_{1-x} Glasses. II. Synthesis Conditions and Defect Formation. *J. Non-Cryst. Solids* **1992**, *146*, 285−293.
(79) Chen, P.; Holbrook, C.; Boolchand, P.; Georgiev, D.; Jackson, K.; Micoulaut, M. Intermediate Phase, Network Demixing, Boson and Floppy Modes, and Compositional Trends in Glass Transition Temperatures of Binary As_xS_{1-x} System. *Phys. Rev. B* **2008**, *78*, 224208.
(80) Qu, T.; Boolchand, P. Shift in Elastic Phase Boundaries Due to Nanoscale Phase Separation in Network Glasses: The Case of $Ge_xAs_xS_{1-2x}$. *Philos. Mag.* **2005**, *85*, 875−884.

■ NOTE ADDED IN PROOF

The phase boundary of the IP in the present Ge_xS_{100-x} binary (Figure 5) as in corresponding selenides (refs 9, 13, 40), and the Ge_x (As or P)$_x$Se$_{100-2x}$ ternaries (Qu, T., et al. *Mater. Res. Soc. Symp. Proc.* **2003**, *754*, 111−122; Chakravarty, S., et al. *J. Phys. Condens. Matter* **2005**, *17*, L1−L7) were each fixed by establishing (i) the variation of the CS mode frequency, $\nu_{cs}(\langle r \rangle)$ in Raman scattering. Even though these measurements are made at discrete glass compositions, one can uniquely establish the *stress* and *rigidity* transitions at fractional compositions as discussed here and elsewhere. (ii) Furthermore, optical elastic power-laws are observed in IPs ($p \sim 1.0$) and stressed-rigid ($p = 1.4 \sim 1.5$) phases with universal values. (iii) IP networks compact and usually display molar volume minima established by measuring density using Archemedes' principle. (iv) Finally, a prerequisite to observing the topology driven elastic phases is that bulk glasses must be homogeneous, as illustrated in the present work, and in molar volume measurements highlighted recently (Bhageria, R., et al.; DOI 10.1002/pssb.201350165). None of these (i−iv) issues were apparently recognized in a recent publication in the present journal by Wang, et al. (DOI 10.1021/jp412226w), which focused entirely on calorimetric methods.